

# NUMERICAL SIMULATION OF THREE-DIMENSIONAL FLOW AROUND HARBOR DUE TO TSUNAMI USING FAVOR METHOD AND WENO SCHEME

Yuki Kajikawa<sup>1</sup>, Masamitsu Kuroiwa<sup>1</sup> and Naohiro Otani<sup>1</sup>

In this paper, a three-dimensional (3D) tsunami flow model was proposed in order to predict a 3D flow field around a harbor accurately when tsunami strikes. In the proposed numerical model, the Cartesian coordinate system was adopted, and the Fractional Area/Volume Obstacle Representation (FAVOR) method, which has the ability to impose boundary conditions smoothly at complex boundaries, was introduced into the governing equations in consideration of applying the estimation to actual harbors with complex shape in the future. Moreover, the fifth-order Weighted Essentially Non-Oscillatory (WENO) scheme, which is a technique for achieving high accuracy even if the calculation mesh is coarse, was applied to discretization of the convection terms of the governing equations. In order to verify the validity of the model, it was applied to a large-scale laboratory experiment with a scale model of harbor. Comparisons between the simulated and experimental results showed that the model was able to reproduce the time variation of the flow field with sufficient accuracy. Moreover, the simulated results showed that a complex 3D flow field with some vertical vortex flows was generated around a harbor when tsunami struck.

*Keywords: Tsunami; harbor; 3D model; numerical simulation; FAVOR method; WENO scheme*

## INTRODUCTION

Topography change around a harbor caused by tsunami affects serious damage to harbor functions, such as the damage to the harbor facilities owing to scouring or the use restriction of ships owing to sediment deposition. Therefore, it is extremely important to evaluate the topography change around a harbor due to tsunami quantitatively in advance. Numerous studies on the topography change due to tsunami have been conducted so far. In particular, there are many studies using a two-dimensional (2D) nonlinear long-wave model for the calculation of tsunami propagation to estimate the topography change (Takahashi et al. 2000, Li and Huang 2012, Sugawara et al. 2014, Kajikawa and Kuroiwa 2017). This is seemingly because that the 2D model is practical and exceedingly useful for the calculation of large-area. However, since the 2D model assumes hydrostatic pressure with vertical velocity 0, it cannot reproduce the topography change such as local scouring around structures.

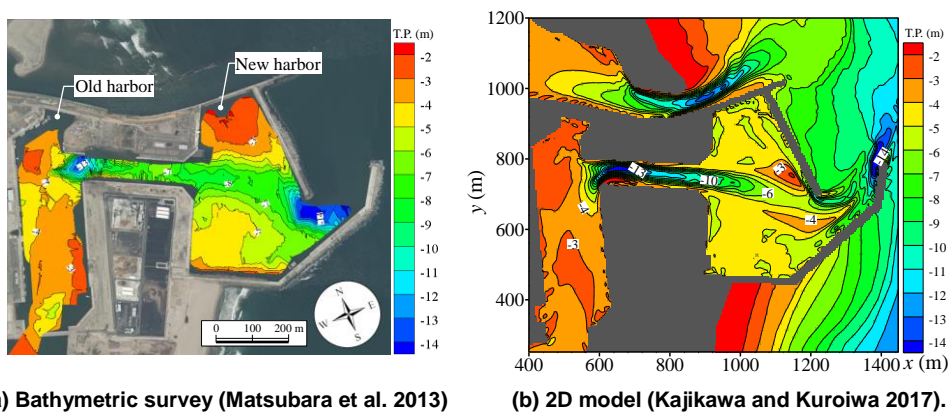


**Figure 1. Comparison between bathymetric survey and 2D model result on topography change around the Yuriage harbor due to the 2011 off the Pacific coast of Tohoku Earthquake Tsunami.**

Fig. 1 shows a comparison between (a) bathymetric survey (Matsubara et al. 2013) and (b) 2D simulated result (Kajikawa and Kuroiwa 2017) on topography change around the Yuriage harbor located at Miyagi prefecture in Japan due to the 2011 off the Pacific coast of Tohoku Earthquake Tsunami. Although the 2D model could reproduce the erosion in the channel connecting the old harbor and the new one, it was not able to reproduce the local scouring at the tip of breakwater. The reason why the local scouring was not reproduced by the 2D model is that a three-dimensional flow field with vertical flow may have been generated in front of the breakwater when tsunami struck. In order to reproduce the local scouring accurately, numerical simulation by using a full three-dimensional (3D) flow model is indispensable.

<sup>1</sup> Graduate School of Engineering, Tottori University, Minami 4-101, Koyama-cho, Tottori, 680-8550, Japan

Recently, several 3D models for the calculation of tsunami propagation have been proposed (Gelfenbaum et al. 2007, Aposos et al. 2011), and the application of these 3D models to large-scale actual topography change are also advancing. However, at present, there are few studies on 3D numerical simulation for flow and local scouring around structures due to tsunamis. This is seemingly because that the calculation time and the domain become enormous in the 3D numerical simulation considering non-hydrostatic pressure.

Incidentally, in the conventional models, first-order upwind scheme has been well used for the discretization of the convection terms of the momentum equations. The first-order upwind scheme is stable discretization method and also easy to program. However, this scheme has a possibility that the prediction accuracy decreases owing to the numerical diffusion if the calculation mesh is coarse. In order to avoid the decrease of the prediction accuracy, application of high-order schemes is effective (Shu 2003). In this study, the authors considered that the application of the fifth-order Weighted Essentially Non-Oscillatory (WENO) scheme (Jiang and Shu 1996, Shu 2003) to discretization of the convection terms. The WENO scheme is a technique for achieving high order accuracy and can calculate discontinuous flows such as shock waves stably. Therefore, a model applied the WENO scheme has a possibility of being able to predict the 3D flow field around structures with stable and high accuracy even if the calculation mesh is coarse.

Moreover, since the topography elevation data or the other statistical data have been arranged in the Cartesian coordinate system so far, the adoption of the Cartesian coordinate system is exceedingly advantageous when model developing. However, solid wall boundaries with complex shape such as a harbor are represented step-wise in this coordinate system. Thereupon the authors considered that the introducing of the Fractional Area/Volume Obstacle Representation (FAVOR) method (Hirt and Sicilian 1985) into the proposed model. The FAVOR method can impose boundary conditions smoothly at complicated boundaries in the Cartesian coordinate system. Therefore, a model into which introduced the FAVOR method has a possibility of being able to calculate flow smoothly along the harbor shape even if the harbor shape is not along this coordinate system.

According to the above, in order to predict a flow and local scouring around structures due to tsunami finally, a full 3D tsunami flow model using the FAVOR method and the WENO scheme was proposed in this paper as a preceding stage. The validity of the proposed model was examined by the application of the model to a large-scale experiment with a scale model of harbor conducted by Fujii et al. (2009).

## NUMRICAL MODEL

### Governing Equations

In the presented numerical model, the 3D Reynolds-Averaged Navier-Stokes equations were used for the calculation of tsunami propagation. The Cartesian coordinate system was adopted in this model, and the FAVOR method (Hirt and Sicilian 1985) with its ability to impose the boundary conditions smoothly at complex boundaries such as harbor shape was introduced into the governing equations. In the FAVOR method, it is assumed that both fluid and boundary exist in an arbitrary lattice. If the volume fraction is occupied by fluid, the volume porosity of the flow region at an arbitrary point is defined  $V$ , if the fraction of area, the area porosity in a cross-section perpendicular to the  $x$ -direction is defined  $A_x$ . The same goes for the  $y$ -direction and  $z$ -direction. Moreover, the linear  $k$ - $\varepsilon$  turbulence model was adopted for the evaluation of the eddy viscosity coefficient. The governing equations introduced with the FAVOR method in the Cartesian coordinate system are denoted by the following equations:

$$\frac{\partial}{\partial x_m} \{A_{(m)} u_m\} = 0 \quad (1)$$

$$\frac{\partial u_l}{\partial t} + \frac{1}{V} \left\{ \frac{\partial A_{(m)} u_m u_l}{\partial x_m} \right\} = -g \delta_{3l} - \frac{1}{\rho} \frac{\partial P}{\partial x_l} + \frac{1}{V} \frac{\partial}{\partial x_m} \left\{ A_{(m)} (v + v_l) \left( \frac{\partial u_l}{\partial x_m} + \frac{\partial u_m}{\partial x_l} \right) \right\} \quad (2)$$

$$\frac{\partial k}{\partial t} + \frac{1}{V} \left\{ \frac{\partial A_{(m)} u_m k}{\partial x_m} \right\} = \frac{1}{V} \frac{\partial}{\partial x_m} \left\{ A_{(m)} V_k \frac{\partial k}{\partial x_m} \right\} + v_l \frac{\partial u_l}{\partial x_m} \left( \frac{\partial u_l}{\partial x_m} + \frac{\partial u_m}{\partial x_l} \right) - \varepsilon \quad (3)$$

$$\frac{\partial \varepsilon}{\partial t} + \frac{1}{V} \left\{ \frac{\partial A_{(m)} u_m \varepsilon}{\partial x_m} \right\} = \frac{1}{V} \frac{\partial}{\partial x_m} \left\{ A_{(m)} V_\varepsilon \frac{\partial \varepsilon}{\partial x_m} \right\} + C_1 \frac{\varepsilon}{k} v_l \frac{\partial u_l}{\partial x_m} \left( \frac{\partial u_l}{\partial x_m} + \frac{\partial u_m}{\partial x_l} \right) - C_2 \frac{\varepsilon^2}{k} \quad (4)$$

$$v_t = C_\mu \frac{k^2}{\varepsilon} \quad (5)$$

$$v_k = v + \frac{v_t}{\sigma_k}, \quad v_\varepsilon = v + \frac{v_t}{\sigma_\varepsilon} \quad (6)$$

where,  $t$  is the time;  $l = 1, 2, 3$ ;  $m = 1, 2, 3$ ;  $(x_1, x_2, x_3) = (x, y, z)$  in the Cartesian coordinates ( $x, y$  and  $z$  denote the horizontal, cross and vertical coordinate respectively in this study);  $u_m$  is the velocity in  $x_m$  direction [ $(u_1, u_2, u_3) = (u, v, w)$ ];  $V$  is the fractional volume rate;  $A_{(m)}$  is the fractional area rate in  $x_m$  direction [ $(A_{(1)}, A_{(2)}, A_{(3)}) = (A_x, A_y, A_z)$ ];  $g$  is the gravitational acceleration;  $\delta$  is the Kronecker's delta;  $\rho$  is the fluid density;  $P = p + 2/3k$ ;  $p$  is the pressure;  $\nu$  is the kinematic viscosity of fluid;  $k$  is the turbulent kinetic energy;  $\varepsilon$  is the turbulent dissipation rate; and  $\nu_t$  is the eddy viscosity coefficient.

The following standard values were used for each constant in the  $k$ - $\varepsilon$  turbulence model:

$$C_\mu = 0.09, \quad \sigma_k = 1.00, \quad \sigma_\varepsilon = 1.30, \quad C_1 = 1.44, \quad C_2 = 1.92 \quad (7)$$

### Numerical Procedure

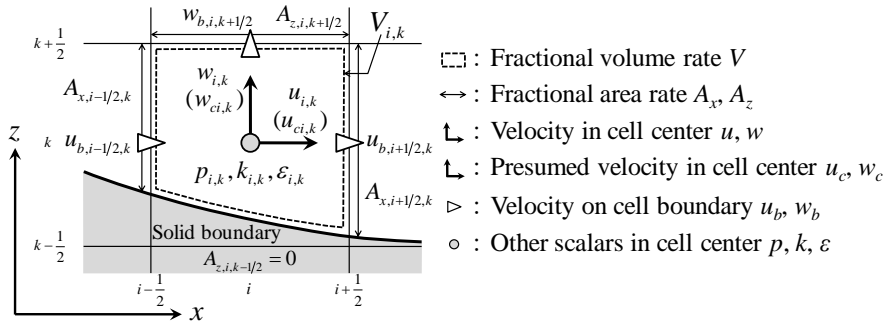


Figure 2. Definition of calculating points on the  $x$ - $z$  plane.

Numerical procedure was almost the same as the C-HSMAC method on the collocated grid arrangement proposed by Ushijima and Nezu (2002). The definition of the calculating points on the  $x$ - $z$  plane is shown in Fig. 2. The numerical procedure was as follows; First, the pressure  $p$  was divided into the static pressure  $p_0$  and the anomaly pressure  $p'$ , and the presumed velocity in the cell center  $u_c(w_c)$  was calculated by the momentum equations Eq. (2) from which the anomaly pressure term was excluded. The WENO scheme and the Adams-Bashforth method were applied to discretization of the momentum equations. Next, the presumed velocity on the cell boundary  $u_b(w_b)$  was calculated by linear interpolation using the presumed velocity in the cell center  $u_c(w_c)$ , and both the new anomaly pressure  $p'$  and the new velocity on the cell boundary  $u_b(w_b)$  were solved by the HSMAC method. Then, the new velocity in the cell center  $u(w)$  was calculated from the presumed velocity in the cell center  $u_c(w_c)$  using the central difference value of the new anomaly pressure  $p'$ . Finally, by using the new velocity on the cell boundary  $u_b(w_b)$ , the new water surface position was calculated from the two-dimensional horizontal continuity equation in which Eq. (1) was integrated in the vertical direction. Moreover, the Hybrid scheme (Spalding 1972) was applied to both convection and diffusion terms of Eq. (3) and Eq. (4).

### Discretization of Convection Term Using WENO Scheme

In the presented numerical model, the fifth-order WENO scheme (Jiang and Shu 1996, Shu 2003) was applied to discretization of the convection terms of the momentum equations Eq (2). However, the third-order WENO scheme and the first-order upwind scheme were applied locally near the water surface and the solid wall boundaries. In the following, the discretization method of the  $x$ -direction convection term using the fifth-order WENO scheme is described:

$$\frac{1}{V} \frac{\partial (A_x u u)}{\partial x} = \frac{A_{x,i+1/2} u_{b,i+1/2} \tilde{u}_{i+1/2} - A_{x,i-1/2} u_{b,i-1/2} \tilde{u}_{i-1/2}}{V_i} + O(\Delta x^5) \quad (8)$$

where,  $u_b$  is the cell boundary velocity calculated by the HSMAC method; and  $\tilde{u}$  is the cell boundary velocity interpolated by the WENO scheme.

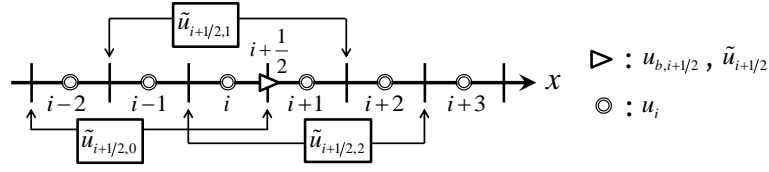


Figure 3. Schematic of computing cell boundary velocity by fifth-order WENO scheme.

Fig. 3 illustrates a schematic of computing cell boundary velocity  $\tilde{u}_{i+1/2}$  by the fifth-order WENO scheme when  $u_{b,i+1/2} \geq 0$ . In the fifth-order WENO scheme, five cell center velocities are needed to estimate one cell boundary velocity. The cell boundary velocity  $\tilde{u}_{i+1/2}$  is calculated as follows:

$$\tilde{u}_{i+1/2} = \sum_{s=0}^2 \omega_s \tilde{u}_{i+1/2,s} \quad (9)$$

$$\tilde{u}_{i+1/2,0} = \frac{1}{3}u_{i-2} - \frac{7}{6}u_{i-1} + \frac{11}{6}u_i \quad (10)$$

$$\tilde{u}_{i+1/2,1} = -\frac{1}{6}u_{i-1} + \frac{5}{6}u_i + \frac{1}{3}u_{i+1} \quad (11)$$

$$\tilde{u}_{i+1/2,2} = \frac{1}{3}u_i + \frac{5}{6}u_{i+1} - \frac{1}{6}u_{i+2} \quad (12)$$

$$\omega_s = \alpha_s / \sum_{f=0}^2 \alpha_f \quad (s = 0, 1, 2) \quad (13)$$

$$\alpha_0 = 0.1/(e + \beta_0)^2, \quad \alpha_1 = 0.6/(e + \beta_1)^2, \quad \alpha_2 = 0.3/(e + \beta_2)^2 \quad (14)$$

$$\beta_0 = \frac{13}{12}(u_{i-2} - 2u_{i-1} + u_i)^2 + \frac{1}{4}(u_{i-2} - 4u_{i-1} + 3u_i)^2 \quad (15)$$

$$\beta_1 = \frac{13}{12}(u_{i-1} - 2u_i + u_{i+1})^2 + \frac{1}{4}(u_{i-1} - u_{i+1})^2 \quad (16)$$

$$\beta_2 = \frac{13}{12}(u_i - 2u_{i+1} + u_{i+2})^2 + \frac{1}{4}(3u_i - 4u_{i+1} + u_{i+2})^2 \quad (17)$$

where,  $e$  is the coefficient to avoid division by zero. In this study,  $e$  was set to  $1.0 \times 10^{-20}$ .

When  $u_{b,i+1/2} < 0$ , the cell boundary velocity  $\tilde{u}_{i+1/2}$  can be calculated by the same equations in consideration of symmetry.

### Boundary Conditions

As the offshore boundary condition, the time variation of water level generated in the target experiment was given. The wall function based on the logarithmic velocity distribution and the assumption of local equilibrium of turbulence was imposed at the solid wall boundary. The free-slip condition for  $u$ ,  $v$  and  $k$  was applied at the water surface boundary. Moreover, the dissipation rate at the water surface  $\varepsilon_s$  was given by the followed formula proposed by Sugiyama et al. (1997):

$$\varepsilon_s = \frac{C_\mu^{3/4} k_s^{3/2}}{\kappa z'} \quad (18)$$

where,  $k_s$  is the turbulent kinetic energy at the water surface;  $\kappa$  is the Von Karman constant ( $= 0.41$ ); and  $z'$  is the distance from the center of the cell adjoining the water surface.

**MODEL APPLICATION**

**Outline of Target Experiment**

In order to verify the validity of the presented model, the authors applied it to an experiment conducted by Fujii et al. (2009). Fig. 4 and Table 1 show the outline of the experimental wave basin and the experimental conditions, respectively. In the experiment, a large-scale basin with 58.0 m length and 20.0 m width was used and a scale model of harbor with 1/100 was installed in the basin. The initial flow depth was set to 0.08 m and a tsunami with half of 60 seconds period and 0.06 m half-amplitude was generated. The height of breakwaters was the height which the generated tsunami did not overflow.

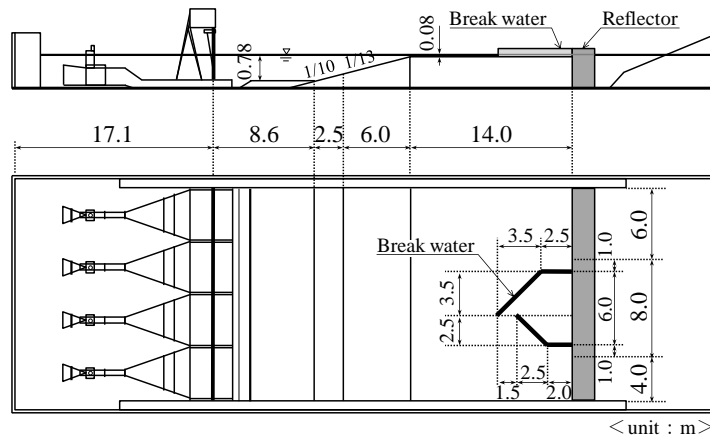


**Figure 4. Experimental wave basin (Fujii et al. 2009).**

**Table 1. Experimental conditions (Fujii et al. 2009).**

Thickness of breakwater	0.15 m
Initial flow depth	0.08 m
Generated tsunami condition	30 sec, 0.06 m

**Calculation Conditions**

Table 2 shows the calculation conditions. In the calculation, horizontal grid sizes  $\Delta x$  and  $\Delta y$  were set to 0.10 m, and vertical grid size  $\Delta z$  was set to 0.02 m. The calculation time step  $\Delta t$  was set to 0.02 seconds and the Manning’s roughness coefficient  $n$  was set to 0.012 sec/m<sup>1/3</sup>. Fig. 5 illustrates the calculation mesh around the harbor. As shown in this figure, since the horizontal grid sizes differed from the thickness of breakwater, the breakwater was represented by using the FAVOR method. Moreover, the authors also carried out the comparisons between the presented model and first-order upwind scheme model in order to confirm the effectiveness of the WENO scheme.

**Table 2. Calculation conditions.**

Calculation time step $\Delta t$	0.02 sec
Horizontal grid size $\Delta x, \Delta y$	0.10 m
Vertical grid size $\Delta z$	0.02 m
Manning’s roughness coefficient $n$	0.012 sec/m <sup>1/3</sup>

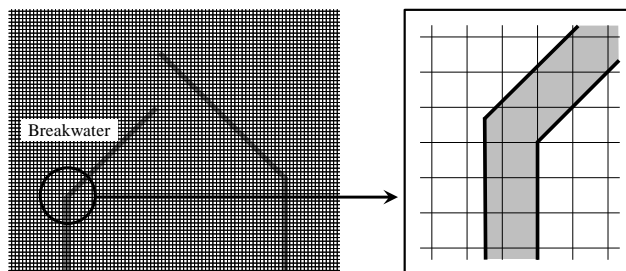


**Figure 5. Calculation mesh around harbor.**

## RESULTS AND DISCUSSION

## Time Variation of Water Surface

Fig. 6 shows the time variation of bird's-eye view of water surface simulated by the presented WENO scheme model. The upper figures in Fig. 6 show the situations at the time of leading wave of tsunami, and the lower figures show the situations at the time of backwash. In the leading wave process of tsunami, the outside water level of the harbor is rising higher than the inside one, and a circulation flow is generated in the center of the harbor. At the time of backwash process, the outside water level of the harbor is decreasing lower than the inside one, and the outflow from the harbor entrance is occurring. Moreover, by using full 3D model, dispersive waves at the front of tsunami are reproduced.

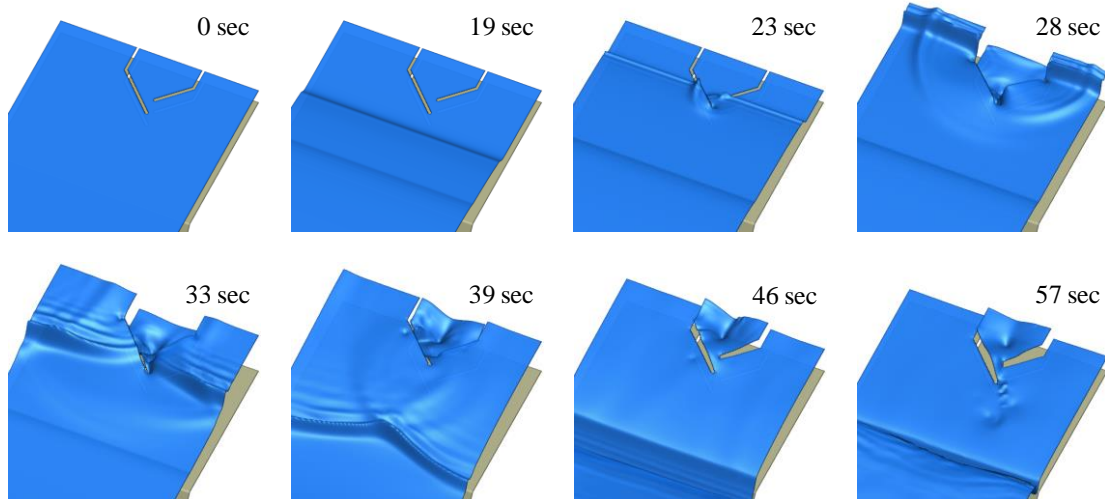


Figure 6. Time variation of bird's-eye view of water surface by the presented WENO scheme model (Upper: Leading wave of tsunami, Lower: Backwash of tsunami).

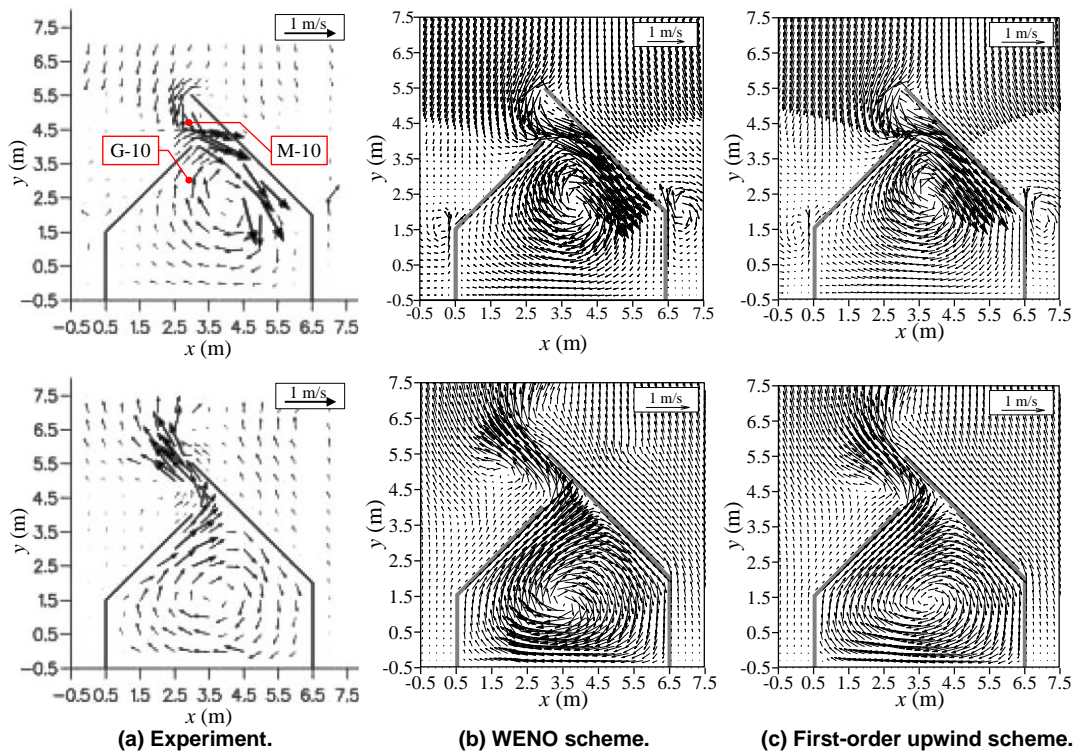


Figure 7. Comparisons between measured and simulated depth-averaged flow velocities (Upper: Leading wave of tsunami, Lower: Backwash of tsunami).

### Comparisons of Flow Velocity Vectors

Fig. 7 shows the depth-averaged flow velocity vectors by (a) experiment, (b) the presented WENO scheme model and (c) the first-order upwind scheme model. The upper figures and the lower figures in Fig. 7 show the situations at the time of the leading wave of tsunami and the backwash of tsunami, respectively. Comparisons of these figures indicate that both numerical models reproduce the experimental flow situations overall. Moreover, the simulated flows in the vicinity of the breakwaters which were installed obliquely for the Cartesian coordinate system are reproduced smoothly along the breakwaters by introducing the FAVOR method. However, by comparing between the WENO scheme and the first-order upwind scheme, the circulation flow velocity in the harbor at the both processes is reproduced stronger in the WENO scheme than the first-order upwind scheme. Furthermore, in terms of the outflow from the harbor entrance at the backwash process, the flow calculated by the first-order upwind scheme tends to more diffuse than the flow by the WENO scheme. Namely, the tendency of the diffusion can be reduced in the WENO scheme since it is a high-order scheme.

### Comparisons of Time Variations of Water Level and Flow Velocities

Fig. 8 and Fig. 9 show comparisons of time variations of water level, velocity  $U$  in the offshore direction and velocity  $V$  in the cross-shore direction by the experiment and the simulations at M-10 and G-10, respectively. M-10 and G-10 are indicated in Fig. 7. Although the calculated flow velocities  $V$  by both numerical models are approximately 0.5 m/s large from the measured value from 30 to 40 seconds at M-10, the calculated results are in good agreement with the measured ones overall. In particular, in regards to the flow velocity  $U$  at M-10, the calculated result by the WENO scheme is better agreement with the experimental data than the first-order upwind scheme.

From the results mentioned above, the validity of the presented WENO scheme model was confirmed.

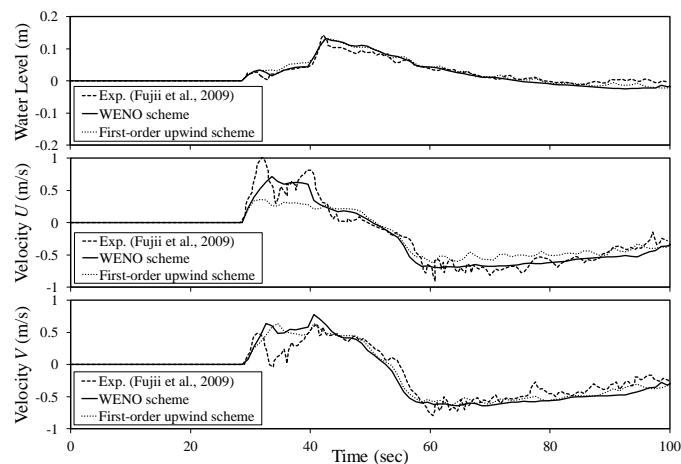


Figure 8. Comparisons of time variations of water level and velocities at M-10 indicated in Fig. 7 (Upper: Water level, Middle: Velocity  $U$ , Lower: Velocity  $V$ ).

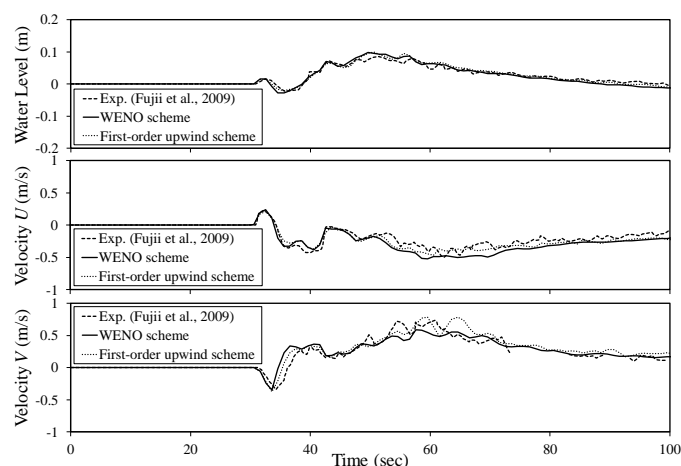


Figure 9. Comparisons of time variations of water level and velocities at G-10 indicated in Fig. 7 (Upper: Water level, Middle: Velocity  $U$ , Lower: Velocity  $V$ ).

## Three-Dimensional Flow Structure around Harbor

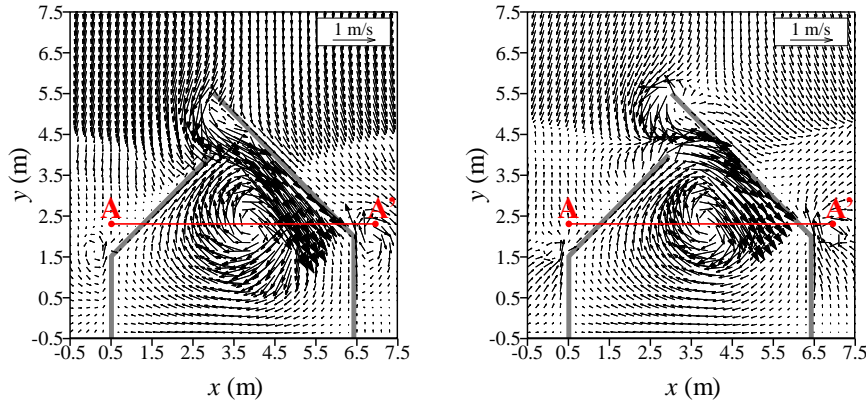


Figure 10. Calculated flow velocity vectors at the time of the leading wave of tsunami (Left: water surface, Right: near-bed).

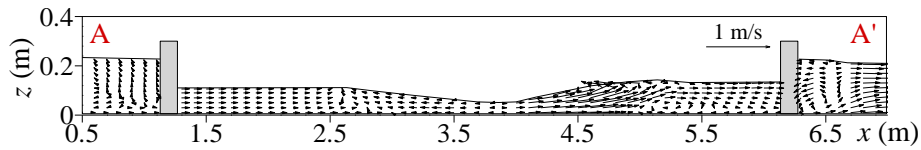


Figure 11. Calculated flow velocity vectors in line A-A' ( $y = 2.4$  m) indicated in Fig. 10.

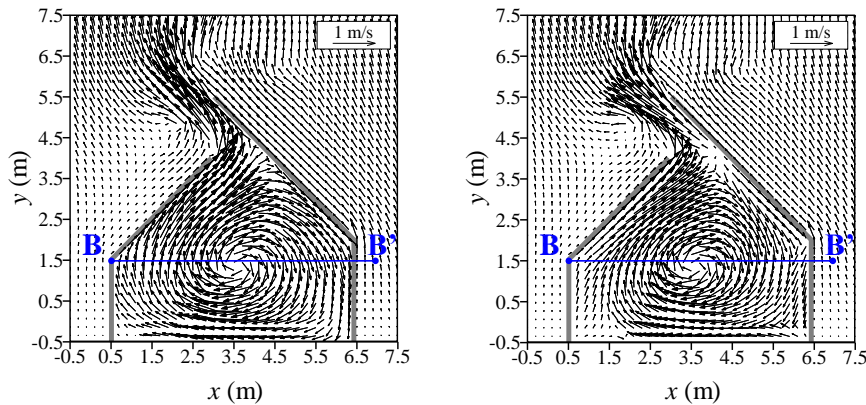


Figure 12. Calculated flow velocity vectors at the time of the backwash of tsunami (Left: water surface, Right: near-bed).

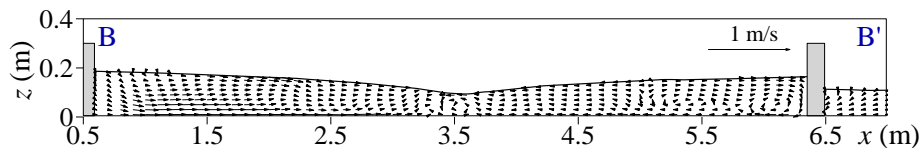


Figure 13. Calculated flow velocity vectors in line B-B' ( $y = 1.5$  m) indicated in Fig. 12.

Fig. 10 shows the calculated flow velocity vectors on the horizontal plane by the presented WENO model at the time of leading wave of tsunami. The left and right figures of Fig. 10 show the situations at the water surface and the near-bed, respectively. The separation flow at the tip of the right-side breakwater is reproduced stronger at the near-bed than the water surface. Moreover, the scale of the circulation flow in the harbor differs between the water surface and the near-bed, and the flow at the water surface is stronger than the near-bed. Fig. 11 shows the calculated flow velocity vectors on the vertical plane in line A-A' ( $y = 2.4$  m) indicated in Fig. 10. Some vertical vortex flows are generated in the harbor ( $x = 5$  m) and near breakwaters, and the flow direction of the water surface differs from one of the near-bed

there. These results indicate that a complex 3D flow field is generated around a harbor when tsunami strikes and a 3D model is indispensable to estimate the topography change.

Fig. 12 shows the calculated flow velocity vectors by the presented WENO model on the horizontal plane at the time of backwash of tsunami. The circulation flow in the harbor is flowing toward the center of the vortex at the near-bed more than the water surface because of the development of the Ekman layer. Moreover, the outflow from the harbor entrance is more spreading at the near-bed than the water surface. Fig. 13 shows the calculated flow velocity vectors on the vertical plane in Line B-B' ( $y = 1.5$  m) indicated in Fig. 12. The horizontal flow velocities in  $x = 1.5$  m are significantly different between the water surface and the near-bed, and a vertical vortex is formed near the right-side breakwater.

Thus, complex 3D flows are generated around a harbor when tsunami strikes and the presented 3D model was able to reproduce such complex flows.

## CONCLUSIONS

This paper proposed a full three-dimensional tsunami flow model using both the FAVOR method and the WENO scheme was proposed in order to predict 3D flow field around a harbor accurately when tsunami strikes. The proposed 3D model was applied to a large-scale experiment with a scale model of harbor conducted by Fujii et al. (2009). The calculated results clarified that the proposed model can simulate flows around structures which are not along the coordinate smoothly by introducing the FAVOR method. Moreover, by comparing between experimental and calculated results, it was confirmed that the proposed WENO numerical model can reproduce the flow field more accurately than the low-order scheme model. In the future work, the authors will introduce a topography change model into this model.

## REFERENCES

- Apotsos, A., Buckley, M., Gelfenbaum, G., Jaffe, B. and Vatvani, D. 2011. Nearshore tsunami inundation model validation: toward sediment transport applications, *Pure and Applied Geophysics*, 168, 2097-2119.
- Fujii, N., Ikeno, M., Sakakiyama, T., Matsuyama, M., Takao, M. and Mukohara, T. 2009. Hydraulic experiment on flow and topography change in harbor due to tsunami and its numerical simulation, *J. Japan Society of Civil Eng.*, B2-65 (1), 291-295 (in Japanese with English abstract).
- Gelfenbaum, G., Vatvani, D., Jaffe, B. and Dekker, F. 2007. Tsunami inundation and sediment transport in vicinity of coastal mangrove forest, *Coastal Sediments 07*, 2, 1117-1128.
- Hirt, C. W. and Sicilian, J. M. 1985. A porosity technique for the definition obstacle in rectangular cell meshes, *Proc. 4th Int. Conf. Numerical Ship Hydrodynamics*, Washington, D.C., 1-19.
- Jiang, G.-S. and Shu, C.-W. 1996. Efficient Implementation of Weighted ENO Schemes, *J. Comput. Phys.*, 126 (1), 202-228.
- Kajikawa, Y. and Kuroiwa, M. 2017. Numerical Simulation of 2D topography change in harbor due to tsunami using high order WENO scheme, *Proc. 9th Int. Conf. APAC 2017*, 527-538.
- Li, L., Qiu, Q. and Huang, Z. 2012. Numerical modeling of the morphological change in Lhok Nga, west Banda Aceh, during the 2004 Indian Ocean tsunami: understanding tsunami deposits using forward modeling method, *Natural Hazards*, 64, 1549-1574.
- Matsubara, Y., Kuroiwa, M., Shibutani, Y., Ichimura, Y. and Yonemura, S. 2013. Damage investigation of the Pacific coast of Tohoku Earthquake Tsunami in the Yuriage harbor using small side scan sonar, *68th Annual Conference of Japan Society of Civil Engineers*, II-185, 369-370 (in Japanese).
- Shu, C.-W. 2003. High order finite difference and finite volume WENO schemes and Discontinuous Galerkin methods for CFD, *Int. J. Comput. Fluid Dynamics*, 17 (2), 107-118.
- Spalding, D. B. 1972. A novel finite difference formulation for differential expressions involving both first and second derivatives, *Int. J. Numerical Methods in Eng.*, 4, 551-559.
- Sugawara, D., Goto, K. and Imamura, F. 2014. Sediment transport due to the 2011 Tohoku-oki tsunami at Sendai: Results from numerical modeling, *Marine Geology*, 358, 18-37.
- Sugiyama, H., Akiyama, M., Kamezawa, M., and Nobuchi, D. 1997. The numerical study of turbulent structure in compound open channel flow with variable depth floodplain, *J. Hydraul, Coastal, Env. Eng., JSCE*, 556 (II-39), 73-83 (in Japanese with English abstract).
- Takahashi, T., Shuto, N., Imamura, F. and Asai, D. 2000. Modeling sediment transport due to tsunami with exchange rate between bedload layer and suspended load layer, *Proc. Int. Conf. Coastal Eng. 2000*, 1508-1519.
- Ushijima, S. and NEZU, I. 2002. Computational method for free-surface flows on collocated grid with moving curvilinear coordinates, *J. Hydraul., Coastal, Env. Eng., JSCE*, 698 (II-58), 11-19 (in Japanese with English abstract).